Chemical Science

ROYAL SOCIETY OF CHEMISTRY

EDGE ARTICLE

View Article Online
View Journal | View Issue

Cite this: *Chem. Sci.*, 2026, **17**, 8021

All publication charges for this article have been paid for by the Royal Society of Chemistry

Received 23rd September 2025
Accepted 20th February 2026

DOI: 10.1039/d5sc07395b

rsc.li/chemical-science

Three wrongs make a right: a computational investigation of [4*n*]–[4*n*]–[4*n*] fused π-systems

Muhammad Usama Gul Khan,[a] Katarzyna Młodzikowska-Pieńko,[b] Renana Gershoni-Poranne *[b] and Judy I. Wu *[a]

Fusing antiaromatic units to other antiaromatic units could afford delocalized [4*n*]–[4*n*]–[4*n*] π-systems with reduced paratropicity (or even weak diatropicity), while retaining narrow HOMO–LUMO gaps. Through a computational investigation of bis-annelated borole-fused cyclobutadiene, pentalene, *s*-indacene, and cyclooctatetraene isomers, we find that these effects are topology-dependent. Comparisons to analogous [4*n* + 2]–[4*n*]–[4*n* + 2] systems show that [4*n*]–[4*n*]–[4*n*] fusion represents a counterintuitive design strategy to access functional antiaromatic π-systems.

Introduction

Ring fusion is a powerful strategy to access π-expanded polycyclic (anti)aromatic hydrocarbons with diverse energetic, magnetic, and electronic properties, and the consequences of fusing [4*n* + 2] to [4*n* + 2] and [4*n*] units have been studied extensively.[1–4] [4*n* + 2]–[4*n* + 2] annelation extends aromaticity; for example, fusing two benzene rings gives naphthalene.[3] In contrast, [4*n* + 2]–[4*n*] fusion weakens both diatropicity in the [4*n* + 2] rings and paratropicity in the [4*n*] rings. For example, in biphenylene, the benzene rings exhibit pronounced bond length alternation while the four-membered ring resembles a [4]radialene.[4,5] As such, [4*n* + 2]–[4*n*]–[4*n* + 2] annelation patterns have emerged as a popular approach for accessing synthetically viable antiaromatic π-systems, as exemplified by preparations of outer and core π-expanded cyclobutadienes,[4,6] pentalenes,[7–10] and *s*-indacenes,[11–13] and extensive studies correlating structure and properties in these systems.[13–16] Yet, the outcomes of combining [4*n*] and [4*n*] units are less intuitive.

In this work, we investigate the effects of [4*n*]–[4*n*]–[4*n*] annelation. We explore whether fusing antiaromatic rings to antiaromatic rings could give rise to overall diatropic (aromatic) compounds while retaining desirable [4*n*] features, such as relatively narrow HOMO–LUMO gaps. The intriguing possibility that [4*n*]–[4*n*] fusion may generate an aromatic π-system with a [4*n* + 2] conjugation pathway was first considered by Breslow in the early 1960s[17–19] and has since attracted much experimental and computational interest.[20–22] Extended Hückel calculations suggest that planar [4*n*]–[4*n*] fused π-systems could exhibit resonance stabilization like the [4*n* + 2] annulenes.[23] Indeed, butalene is planar and displays bond length equalization as well as large negative nucleus-independent chemical shifts (NICS) values, consistent with aromatic character.[24,25] Nevertheless, attempts to prepare cyclooctatetraenocyclopentadienone (COT-CPD) (Fig. 1a),[17] cyclooctatetraenocyclobutadiene (COT-CBD) (Fig. 1b),[26–28] octalene (Fig. 1c and d),[29,30] bicyclotropone (Fig. 1e),[31] and butalene (Fig. 1f)[32,33] generally yielded highly reactive or fleeting species, providing little evidence for aromatic stabilization.

Breslow *et al.* noted that "the high basicity [of COT-CPD] suggests that the bicyclic 10π-electron cation may be aromatic."[17] Proton NMR chemical shifts for COT-CBD (ranging between 6.18–7.32 ppm) were downfield shifted, indicating some diatropicity (Fig. 1b).[28] Yet, ^{1}H NMR chemical shifts for the eight-membered rings of COT-CPD (ranging between 5.50–6.50 ppm)[17] (Fig. 1a) and benzooctalene (5.65–6.30 ppm)[29] (Fig. 1c) are nearly identical to that of cyclooctatetraene (5.69 ppm). Bicyclotropone isomers reflect the intrinsic instability of their [4*n*] subunits rather than the peripheral [4*n* + 2] π-system; the 2-isomer polymerizes at room temperature, while the 1-isomer could not be isolated (Fig. 1e).[31] Butalene could be generated separately from *p*-benzyne and trapped "somewhat below room temperature," but has only fleeting existence

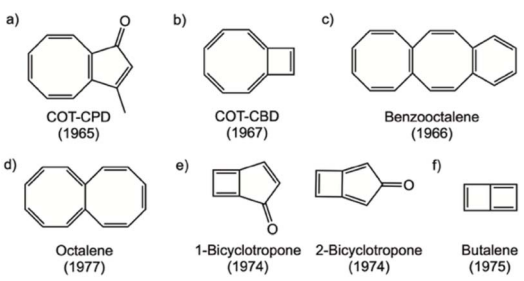

Fig. 1 Synthetic examples of [4*n*]–[4*n*] fused systems: (a) COT-CPD,[17] (b) COT-CBD,[26–28] (c) benzooctalene,[29] (d) octalene,[30] (e) 1-bicyclotropone and 2-bicyclotropone,[31] (f) butalene.[33]

[a]*Department of Chemistry, University of Houston, Houston, Texas, 77204-5003, USA*
[b]*Schulich Faculty of Chemistry, The Resnick Sustainability Center for Catalysis, Technion—Israel Institute of Technology, Haifa 32000, Israel*

(Fig. 1f).[33] We note, however, that all of the examples shown in Fig. 1 contain either a nonplanar cyclooctatetraene unit (which precludes effective π-conjugation) or a strained cyclobutadiene unit[34,35] (which competes with aromatic stabilization).

Here, we investigate the energetic, electronic, and magnetic properties of bis-annelated borole-fused cyclobutadiene, pentalene, *s*-indacene, and cyclooctatetraene isomers. By extending Breslow's original question to [4*n*]–[4*n*]–[4*n*] fused π-systems, we explore a counterintuitive design strategy in which antiaromatic units are fused to other antiaromatic units, rather than stabilized through conventional [4*n* + 2] annelation. We assess whether this largely unexplored region of chemical space can complement existing outer and core π-expanded strategies based on [4*n* + 2] annelation, and provide access to functional antiaromatic π-systems that retain narrow HOMO–LUMO gaps and desirable optoelectronic properties.[36,37]

Results and discussion

We investigated a series of [4*n*]–[4*n*]–[4*n*] bis-annelated borole-fused cyclobutadiene (**1**), pentalene (**2**), *s*-indacene (**3**), and cyclooctatetraene (**4**). We chose borole annelation because the five-membered borole rings are planar and relatively unstrained. Since the borole rings could be fused to the central [4*n*] components in different orientations, we also studied how placement of the boron atoms influences the overall tropicity of the fused π-system.[38–40] We distinguished between molecules in which the boron atom is not adjacent to the fused bond (*terminal*) and those where it is; for the latter case, we further distinguished based on the relative orientation between the two borons (*syn* or *anti*). All structures were optimized at the (U)M11/6-311+G(d,p) level. **3**-*Syn* (y_0 = 0.40) and **3**-*terminal* (y_0 = 0.54) show modest diradicaloid character, while all others exhibit stable closed-shell wavefunctions (see details in the SI).

NICS[41,42] were computed at the (U)B97-2/6-311+G(d,p)//(U)M11/6-311+G(d,p) level to quantify the paratropic character of the annelated four- (4MR), five- (5MR), six- (6MR), or eight- (8MR) membered rings. The B97-2 functional was selected for NMR calculations as it has been shown to have the best performance based on test sets of a broad range of organic compounds.[43] For planar systems, the NICS(1)$_{zz}$ index was applied and bqs were placed at 1 Å above the ring plane. For systems containing cyclooctatetraene subunits, a single NICS(0) value was computed; "0" is defined by the center of mass of the 8MR carbons. We adopted the NICS(0) index in this work to enable direct comparison with NICS(0) values computed for the non-planar species shown in Fig. 1, some of which do not have a defined "*zz*" direction (see data in the SI). NICS(1)$_{zz}$-XY scans[44] were computed for all planar systems, using the NICS(1)$_{zz}$ index; details of the scan paths are included in the SI. Current density plots (generated with the SYSMOIC package),[45] containing only the contributions of the π-orbitals, were computed for all planar systems at 1 Å above the molecular plane at B97-2/6-311+G(d,p). Counter-clockwise currents indicate paratropicity and clockwise currents indicate diatropicity (see SI for details).

Across all four [4*n*] cores examined, a consistent pattern emerges: *syn*- and *anti*-fused topologies enable overlapping [4*n* + 2] circuits that weaken paratropicity of the [4*n*]–[4*n*]–[4*n*] π-system. *Terminal*-fusion precludes a local [4*n* + 2] circuit and therefore gives rise to π-systems with strong paratropicity. Interestingly, all of the borole-fused [4*n*]–[4*n*]–[4*n*] π-systems display notably narrower HOMO–LUMO gaps compared to their dibenzo-fused [4*n* + 2]–[4*n*]–[4*n* + 2] analogs. These findings suggest that [4*n*]–[4*n*]–[4*n*] may represent an alternative design strategy towards functional antiaromatic π-systems.

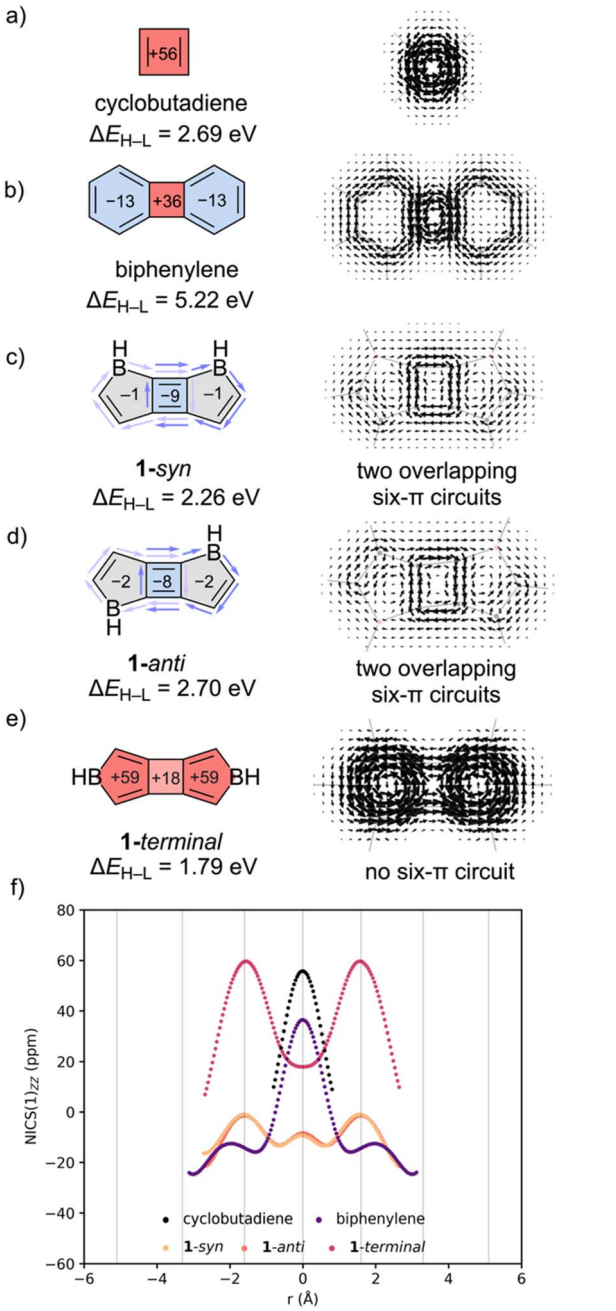

Fig. 2 Computed NICS(1)$_{zz}$, current density plots, and ΔE_{H-L} gaps for (a) cyclobutadiene, (b) biphenylene, (c) **1**-*syn*, (d) **1**-*anti*, (e) **1**-*terminal*. The two overlapping six-π-conjugated circuits in **1**-*syn* and **1**-*anti* are shown in light and dark purple arrows. (f) NICS(1)$_{zz}$-XY scans at B97-2/6-311+G(d,p). The maxima in each curve indicate the ring centers of each annelated ring.

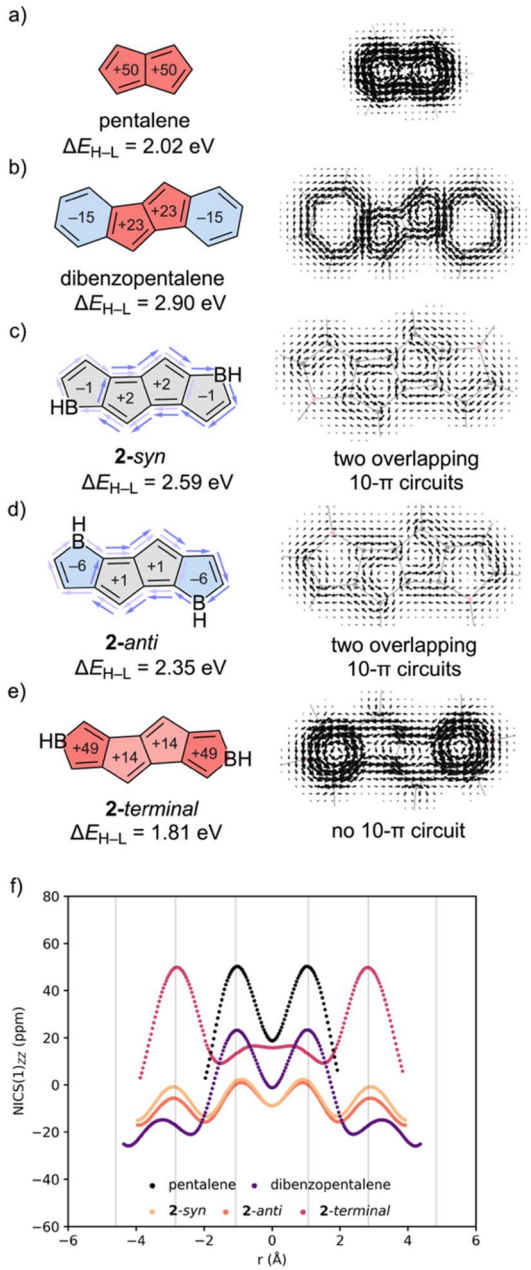

Fig. 3 Computed NICS(1)$_{zz}$, current density plots, and ΔE_{H-L} gaps for (a) pentalene, (b) dibenzopentalene, (c) **2**-*syn*, (d) **2**-*anti*, and (e) **2**-*terminal*. The two overlapping 10-π-conjugated circuits in **2**-*syn* and **2**-*anti* are shown in light and dark purple arrows. (f) NICS(1)$_{zz}$-XY scans at B97-2/6-311+G(d,p). The maxima in each curve indicate the ring centers of each annelated ring.

Computed NICS-XY scans for cyclobutadiene, biphenylene, and the bis-annelated borole-fused cyclobutadiene isomers: **1**-*syn*, **1**-*anti*, and **1**-*terminal* (Fig. 2) reveal that cyclobutadiene is strongly paratropic (Fig. 2f, black curve), while biphenylene displays decreased paratropicity in the 4MR and weak diatropicity in the two 6MRs (purple). Bisborole-fusion in either a *syn*- (peach) or *anti*- (orange) fashion converts the 4MR ring into a modestly diatropic unit, while the two 5MRs become essentially non-aromatic. In **1**-*terminal* (magenta), the 4MR shows reduced paratropicity compared to cyclobutadiene and biphenylene, while the two 5MRs are strongly paratropic.

SYSMOIC plots for cyclobutadiene and biphenylene show local paratropic ring currents around the 4MR and diatropic currents around the 6MR. However, in **1**-*syn* (Fig. 2c) and **1**-*anti* (Fig. 2d), there are two overlapping diatropic currents, each encompassing a 6π-electron perimeter of a pair of neighboring 4MR and 5MRs. The combined effect is an apparent weak diatropic current at the central 4MR (see light and dark purple arrows in Fig. 2c and d). In **1**-*terminal*, an 8π-electron conjugation pathway gives rise to a strong paratropic current around the perimeter.

HOMO–LUMO gaps (ΔE_{H-L}) for the borole-fused isomers were computed at TD-(U)M11/6-311+G(d,p) and compared to the dibenzo-fused [4*n* + 2]–[4*n*]–[4*n* + 2] analogs and parent [4*n*] systems. Surprisingly, all three [4*n*]–[4*n*]–[4*n*] systems, **1**-*syn* (2.26 eV), **1**-*anti* (2.70 eV), and **1**-*terminal* (1.79 eV), exhibit narrower computed ΔE_{H-L} values compared to the [4*n* + 2]–[4*n*]–[4*n* + 2] fused biphenylene (5.22 eV). This can be attributed in part to the low-lying LUMO orbitals of the borole-fused isomers (*i.e.*, due to the empty p orbitals on boron), but nevertheless, demonstrate that heteroatom doping can be used to modulate [4*n*]–[4*n*]–[4*n*] π-systems and show reduced paratropicities while retaining narrow HOMO–LUMO gaps.

We next compared computed NICS-XY scans for pentalene, dibenzopentalene, and isomers: **2**-*syn*, **2**-*anti*, and **2**-*terminal* (Fig. 3). Pentalene is strongly paratropic (Fig. 3f, black). In dibenzopentalene (purple), the 5MRs show reduced paratropicity and the 6MRs are modestly diatropic. Borole-fusion in either a *syn*- (peach) or *anti*- (orange) fashion completely alleviates the paratropicity of the pentalene core, while the fused borole rings are weakly diatropic. In **2**-*terminal* (magenta), the pentalene rings are modestly paratropic and the borole rings are strongly paratropic. These findings corroborate prior work showing that fusion to heteroarenes can significantly alter the paratropicity of pentalene.[46]

SYSMOIC plots for pentalene (Fig. 3a) and dibenzopentalene (Fig. 3b) reveal strong paratropic ring currents around the pentalene unit and local diatropic currents around the 6MR, while those of the borole-fused isomers feature overlapping ring currents. Both **2**-*syn* (Fig. 3c) and **2**-*anti* (Fig. 3d) exhibit weak paratropic circuits at the pentalene core and two overlapping 10π-electron circuits, each encompassing the perimeter of a single borole subunit and its adjacent pentalene core (see light and dark purple arrows in Fig. 3c and d). As a result of these overlapping ring currents, the pentalene core is essentially non-aromatic. In contrast, **2**-*terminal* features a 12π-electron conjugation pathway and a strong paratropic current around the perimeter. All three isomers: **2**-*syn* (2.59 eV), **2**-*anti* (2.35 eV), and **2**-*terminal* (1.81 eV) exhibit narrower ΔE_{H-L} gaps compared to the [4*n* + 2]–[4*n*]–[4*n* + 2] fused dibenzopentalene (2.90 eV).

Next, we compared *s*-indacene and dibenzo-*s*-indacene to the bis-annelated borole-fused: **3**-*syn*, **3**-*anti*, and **3**-*terminal* (Fig. 4). Computed NICS-XY scans show strong diatropicity in the 6MR and 5MRs of *s*-indacene (Fig. 4f, black). In dibenzo-*s*-indacene (purple), the *s*-indacene core shows significantly reduced paratropicity, while the two arenes are modestly diatropic. Bis-

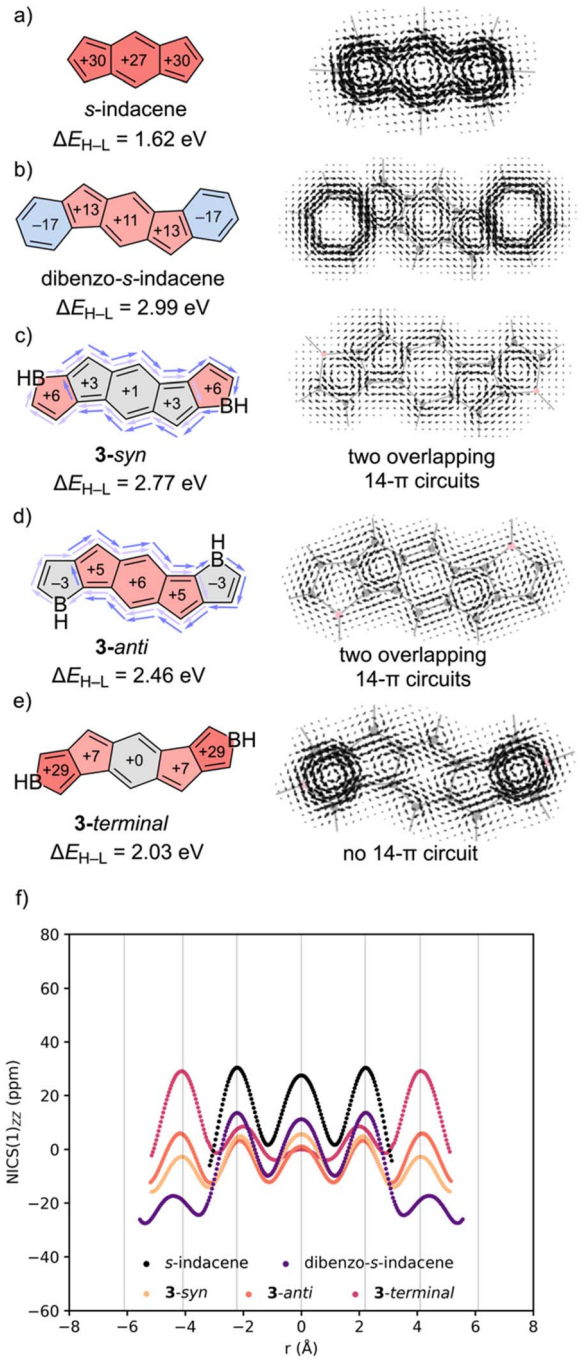

Fig. 4 Computed NICS(1)$_{zz}$, current density plots, and ΔE_{H-L} gaps for (a) *s*-indacene, (b) dibenzo-*s*-indacene, (c) **3**-*syn*, (d) **3**-*anti*, and (e) **3**-*terminal*. The two overlapping 14-π-conjugated circuits in **3**-*syn* and **3**-*anti* are shown in light and dark purple arrows. (f) NICS(1)$_{zz}$-XY scans at (U)B97-2/6-311+G(d,p). The maxima in each curve indicate the ring centers of each annelated ring.

annelation to borole in either a *syn*- or *anti*-fashion further reduces paratropicity of the *s*-indacene core. Both **3**-*syn* (peach) and **3**-*anti* (orange) have nearly non-aromatic borole rings, while that of **3**-*anti* shows weak diatropicity. In **3**-*terminal* (magenta) the *s*-indacene core is essentially non-aromatic, but the two borole rings are strongly paratropic.

SYSMOIC plots reveal a strong global paratropic ring current for *s*-indacene (Fig. 4a), while dibenzo-*s*-indacene exhibits five local ring currents: two diatropic ones around the arenes and three paratropic ones in each of the rings in the *s*-indacene unit (Fig. 4b). Both **3**-*syn* (Fig. 4c) and **3**-*anti* (Fig. 4d) exhibit a weak global diatropic current, and weak paratropic currents in each of the component rings. Also visible from the current density plots are two overlapping 14π-electron circuits, each encompassing the perimeter of a pair of neighboring borole units and the *s*-indacene core (see light and dark purple arrows in Fig. 4c and d). In contrast, **3**-*terminal* features an 18π-electron conjugation pathway and a paratropic current around the perimeter. In addition, the borole rings sustain strong local paratropic ring currents. All three bis-annelated borole-fused isomers: **3**-*syn* (2.77 eV), **3**-*anti* (2.46 eV), and **3**-*terminal* (2.03 eV) exhibit narrower ΔE_{H-L} gaps compared to the [4*n* + 2]–[4*n*]–[4*n* + 2] fused dibenzo-*s*-indacene (2.99 eV), and indicate heteroatom doping as a viable strategy for modulating [4*n*]–[4*n*]–[4*n*] π-systems.

Finally, we examine [4*n*]–[4*n*]–[4*n*] annelated systems with a central cyclooctatetraene (COT) unit (Fig. 5). Planar annelated COTs have been studied extensively, both computationally and experimentally.[47–53] Fusing small, strained rings to COT can enforce planarity,[52] but the paratropicity of the planar COT core depends on the annelated ring(s); annelation to unconjugated units (*e.g.*, bicyclo[2.1.1]hexeno and cyclobuteno) retains the paratropicity of planar COT, while annelation to conjugated units (*e.g.*, cyclobutadieno) quenches paratropicity.[53] Here, we compare dibenzo-COT to three isomers of bis-annelated borole-fused COTs: **4**-*syn*, **4**-*anti*, and **4**-*terminal* (Fig. 5), all of which feature nonplanar COT rings.

Parent COT adopts a nonplanar tub-shape (D_{2d}, ϕ_{1234} = 57.9°) to avoid ring strain and antiaromaticity that are inherent in the planar geometry,[54] and the computed small positive NICS(0) value (+2.4 ppm) is consistent with a non-aromatic ring (Fig. 5). In contrast, planar COT (D_{4h}) exhibits a large positive NICS(0) value (+36.0 ppm) indicating strong paratropicity. Dibenzo-COT retains a highly puckered tub shape (ϕ_{1234} =

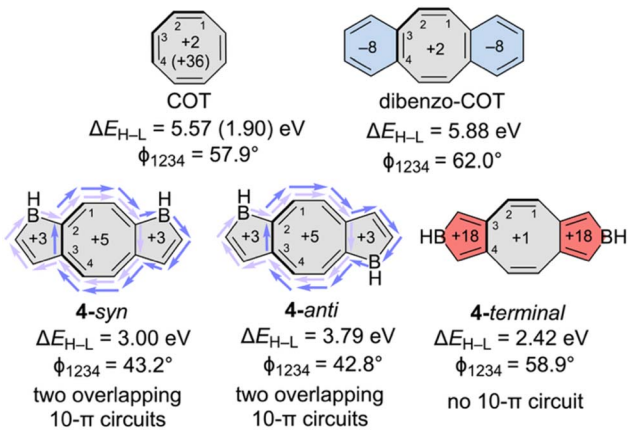

Fig. 5 Computed NICS(1)$_{zz}$, ΔE_{H-L} gaps, and relevant dihedral angles for cyclooctatetraene (data for D_{4h} form is shown in parenthesis), dibenzocyclooctatetraene, **4**-*syn*, **4**-*anti*, and **4**-*terminal*. The two overlapping ten π-conjugated circuits in **4**-*syn* and **4**-*anti* are shown in black and blue arrows.

62.0°), and computed NICS(0) values at the 8MR (+2.1 ppm) and 6MRs (−8.0 ppm, *cf.* −8.3 ppm for parent benzene) suggest a non-aromatic [4*n*] core flanked by two aromatic benzene rings.

Annelating COT to borole units in either a *syn* or *anti* fashion does not fully planarize the COT unit. Nevertheless, both **4**-*syn* and **4**-*anti* tend towards partial planarization exhibiting smaller ϕ_{1234} dihedral angles (43.2° and 42.8°, respectively) compared to dibenzo-COT. Computed NICS(0) values for the component rings in **4**-*syn* (borole unit: +3.0 ppm, COT unit: +4.8 ppm) and **4**-*anti* (borole unit: +2.9 ppm, COT unit: +4.8 ppm) are all small and positive, indicating essentially non-aromatic π-systems. The modestly flattened COT units in **4**-*syn* and **4**-*anti* suggest that some delocalization is possible.

Indeed, previous calculations of current densities for D_{2d} COT geometries, progressively planarized from the tub-shaped parent structure, show that a paratropic ring current "survives almost all the way to the equilibrium tub-shaped D_{2d} COT structure; the current vanishes at ca. 80% of the geometric change."[55] Hence, some delocalization is reasonable to expect for nonplanar **4**-*syn* and **4**-*anti*; specifically, the two overlapping 10π-conjugated circuits (see black and blue arrows in Fig. 5) can provide a driving force for planarization. **4**-*Terminal* does not sustain a 10π-conjugated circuit, and therefore the COT unit is strongly puckered ($\phi_{1234} = 58.9°$) like that of COT and dibenzo-COT. Computed NICS(0) values for **4**-*terminal* indicate a non-aromatic COT unit (+1.2 ppm) flanked by two paratropic borole rings (+17.5 ppm). We note that all three isomers: **4**-*syn* (2.00 eV), **4**-*anti* (3.79 eV), **4**-*terminal* (2.42 eV) have smaller ΔE_{H-L} values compared to dibenzo-COT (5.88 eV).

Computed relative energies for the *syn*-, *anti*-, and *terminal*-isomers of **1–4** (ΔE_{rel}) support the conclusion that π-delocalization strongly stabilizes the *syn*- and *anti*-isomers relative to their *terminal*-analogs. As shown in Table 1, the *syn*- and *anti*-isomers for **2–4** are nearly thermoneutral with respect to one another or have only small relative energy differences, while the *terminal*-analogs lie 10–25 kcal mol^{-1} higher in energy. This trend does not hold for the isomers of **1**, possibly due to strain associated with the 4MR unit. Note that all three isomers of **1** lie within 4 kcal mol^{-1} of each other. The small energy differences among **1**-*syn*, **1**-*anti*, and **1**-*terminal* can be explained by the resonance forms of the 4MR unit. In **1**-*syn* and **1**-*anti*, the π-system is stabilized by having two overlapping [4*n* + 2] circuits, but the central 4MR unit resembles a strained cyclobutadiene. By contrast, in **1**-*terminal*, the central 4MR unit resembles a [4] radialene.

We further studied the nature of the *syn*- and *anti*-fused isomers (relative to terminally fused isomers) by examining plots of their frontier molecular orbitals, by quantifying estimates of π-electron delocalization energies, and by analyzing their bond length alternation around the perimeter. Visualization of the highest occupied molecular orbitals (HOMOs) for the *syn*-, *anti*-, and *terminal*-isomers of **1–4** shows bonding MOs for the *syn*- and *anti*-isomers, which is characteristic of aromatic molecules. In contrast, the HOMOs of the *terminal*-isomers have much more antibonding character (Fig. 6), which is often seen in antiaromatic systems. This contrast is particularly noteworthy in light of the structural similarity between the systems (*i.e.*, same number of atoms, rings, and extent of conjugated systems); it underlines the fundamental difference in electronic structure between the isomers. Further support was obtained from second-order orbital perturbation ($E(2)$) analyses, which quantify donor–acceptor interactions, and reveal consistently higher electron-delocalization energies for the *syn*- and *anti*-isomers compared to the *terminal*-analogs (see Table S1). Finally, from the geometrical aspect, the *syn*- and *anti*-isomers exhibit less pronounced bond length alternation around the perimeter, in agreement with a more globally delocalized π-system (see Fig. S4). These trends are consistent with a largely suppressed antiaromatic character for the *syn*- and *anti*-isomers, relative to the *terminal*-analogs, and demonstrate that the effects of [4*n*]–[4*n*]–[4*n*] fusion are topology-dependent.

Table 1 Computed relative energies (ΔE_{rel}, in kcal mol^{-1}) for the *syn*-, *anti*-, and *terminal*-fused isomers of **1–4**

Compound	ΔE_{rel}	Compound	ΔE_{rel}
1-*Syn*	3.8	**3**-*Syn*	0.0[a]
1-*Anti*	0.0	**3**-*Anti*	2.9
1-*Terminal*	3.0	**3**-*Terminal*	10.9[a]
2-*Syn*	0.8	**4**-*Syn*	0.3
2-*Anti*	0.0	**4**-*Anti*	0.0
2-*Terminal*	10.2	**4**-*Terminal*	24.2

[a] Both **3**-*syn* and **3**-*terminal* have modest diradicaloid character and thus were evaluated with UKS.

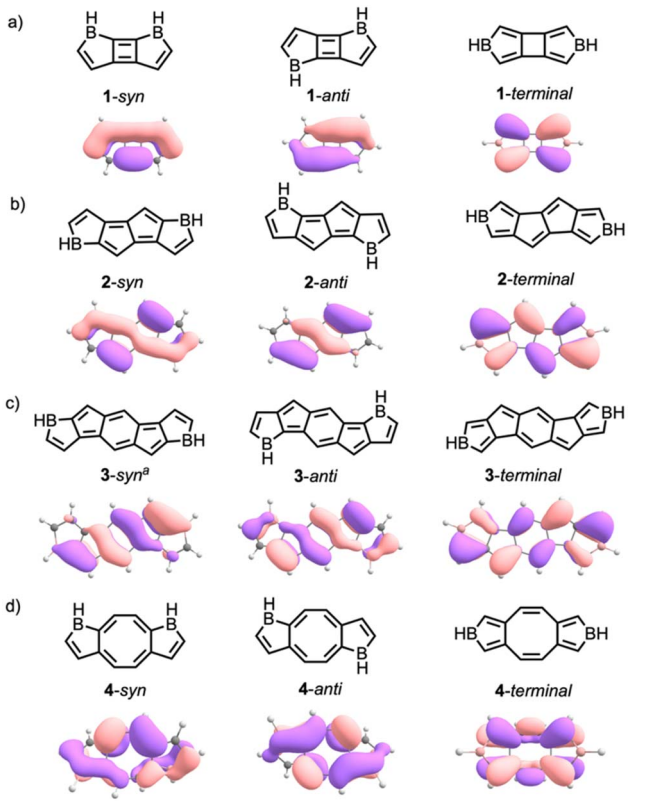

Fig. 6 Computed HOMO ([a]SHOMO−1 for **3**-*syn*) orbitals for the *syn*-, *anti*-, and *terminal*-isomers of **1–4**.

Conclusions

We have systematically investigated [4*n*]–[4*n*]–[4*n*] fused π-systems as an alternative and previously underexplored design strategy for functional antiaromatic molecules. By extending Breslow's original question beyond isolated [4*n*]–[4*n*] fusion to a broader set of topologically-controlled [4*n*]–[4*n*]–[4*n*] π-systems, we demonstrate that strategic bis-annelation of borole rings to cyclobutadiene, pentalene, *s*-indacene, and cyclooctatetraene frameworks can effectively "conceal antiaromaticity,"[2] yielding non-aromatic or weakly aromatic π-systems. Remarkably, these [4*n*]–[4*n*]–[4*n*] π-systems exhibit narrower HOMO–LUMO gaps compared to analogous [4*n* + 2]–[4*n*]–[4*n* + 2] dibenzo-fused systems. Although the presence of the B atoms may play a role, the examples shown in Fig. 1 (which do not contain B atoms) make it clear that the [4*n*]–[4*n*]–[4n] topology itself results in attenuation of the paratropic current. Our computational investigation of [4*n*]–[4*n*]–[4*n*] fused π-systems demonstrates that "three wrongs can make a right"[18] and provides topology-driven design principles that motivate future synthetic efforts in this region of chemical space.

Author contributions

Conceptualization: JW; data curation and formal analysis: MUGK; funding acquisition: JW, RGP; investigation: MUGK, KMP; methodology: MUGK, RGP; project administration and resources: JW, RGP; supervision: JW, RGP; visualization: MUGK; writing – original draft: MUGK; writing – review and editing: MUGK, KMP, RGP, JW. All authors have given approval to the final version of the manuscript.

Conflicts of interest

There are no conflicts of interest to declare.

Data availability

The data supporting this article have been included as part of the supplementary information (SI). Supplementary information is available. See DOI: https://doi.org/10.1039/d5sc07395b.

Acknowledgements

J. I. W. thanks the National Science Foundation (CHE-2303851) for financial support. We acknowledge the use of the Carya and Sabine clusters and support from the Research Computing Data Core at the University of Houston. K. M. P. is grateful to the Azrieli Foundation for financial support through a postdoctoral fellowship. R. G. P. gratefully acknowledges the support of the Israel Science Foundation (Grant #1745/23).

Notes and references

1 E. Vidal Jr., G. I. Warren, J. E. Barker and M. M. Haley, *Chem. Sci.*, 2025, **16**, 19026–19047.
2 F. Glöcklhofer, *Open Res. Eur.*, 2025, **5**, 70.
3 E. Steiner and P. W. Fowler, *Int. J. Quantum Chem.*, 1996, **60**, 609–616.
4 S. Radenković, J. Tošović, R. W. A. Havenith and P. Bultinck, *ChemPhysChem*, 2015, **16**, 216–222.
5 J. Thiele, *Adv. Cycloaddit.*, 1899, **306**, 87–142.
6 W. C. Lothrop, *J. Am. Chem. Soc.*, 1941, **63**, 1187–1191.
7 T. Kawase, T. Fujiwara, C. Kitamura, A. Konishi, Y. Hirao, K. Matsumoto, H. Kurata, T. Kubo, S. Shinamura, H. Mori, E. Miyazaki and K. Takimiya, *Angew. Chem., Int. Ed.*, 2010, **49**, 7728–7732.
8 K. Brand, *Ber. Dtsch. Chem. Ges.*, 1912, **45**, 3071–3077.
9 T. Kawase, A. Konishi, Y. Hirao, K. Matsumoto, H. Kurata and T. Kubo, *Chem.–Eur. J.*, 2009, **15**, 2653–2661.
10 Z. U. Levi and T. D. Tilley, *J. Am. Chem. Soc.*, 2009, **131**, 2796–2797.
11 J. L. Marshall, K. Uchida, C. K. Frederickson, C. Schütt, A. M. Zeidell, K. P. Goetz, T. W. Finn, K. Jarolimek, L. N. Zakharov, C. Risko, R. Herges, O. D. Jurchescu and M. M. Haley, *Chem. Sci.*, 2016, **7**, 5547–5558.
12 D. T. Chase, B. D. Rose, S. P. McClintock, L. N. Zakharov and M. M. Haley, *Angew. Chem., Int. Ed.*, 2011, **50**, 1127–1130.
13 J. Usuba and A. Fukazawa, *Chem.–Eur. J.*, 2021, **27**, 16127–16134.
14 G. I. Warren, K. Młodzikowska-Pieńko, S. Jalife, I. S. Demachkie, J. I. Wu, M. M. Haley and R. Gershoni-Poranne, *Chem. Sci.*, 2025, **16**, 575–583.
15 S. Jalife and J. I. Wu, *J. Org. Chem.*, 2025, **90**, 4012–4017.
16 S. Jalife, A. Tsybizova, R. Gershoni-Poranne and J. I. Wu, *Org. Lett.*, 2024, **26**, 1293–1298.
17 R. Breslow, W. Vitale and K. Wendel, *Tetrahedron Lett.*, 1965, **6**, 365–368.
18 R. Breslow, *Chem. Rec.*, 2014, **14**, 1174–1182.
19 M. E. Vol'pin, *Russ. Chem. Rev.*, 1960, **29**, 129–160.
20 R. Breslow, *Acc. Chem. Res.*, 1973, **6**, 393–398.
21 R. G. Bergman, *Acc. Chem. Res.*, 1973, **6**, 25–31.
22 M. Oda, *Pure Appl. Chem.*, 1986, **58**, 7–14.
23 J. D. Roberts, A. Streitwieser Jr. and C. M. Regan, *J. Am. Chem. Soc.*, 1952, **74**, 4579–4582.
24 P. M. Warner and G. B. Jones, *J. Am. Chem. Soc.*, 2001, **123**, 10322–10328.
25 K. Ohta and T. Shima, *Chem. Phys. Lett.*, 1994, **217**, 7–12.
26 J. A. Elix, M. V. Sargent and F. Sondheimer, *J. Am. Chem. Soc.*, 1967, **89**, 180.
27 G. Schröder and H. Röttele, *Angew Chem. Int. Ed. Engl.*, 1968, **7**, 635–636.
28 M. Oda and H. Oikawa, *Tetrahedron Lett.*, 1980, **21**, 107–110.
29 R. Breslow, W. Horspool, H. Sugiyama and W. Vitale, *J. Am. Chem. Soc.*, 1966, **88**, 3677–3678.
30 E. Vogel, H.-V. Runzheimer, F. Hogrefe, B. Baasner and J. Lex, *Angew. Chem., Int. Ed. Engl.*, 1977, **16**, 871–872.
31 R. Breslow, M. Oda and T. Sugimoto, *J. Am. Chem. Soc.*, 1974, **96**, 1639–1640.
32 R. R. Jones and R. G. Bergman, *J. Am. Chem. Soc.*, 1972, **94**, 660–661.
33 R. Breslow, J. Napierski and T. C. Clarke, *J. Am. Chem. Soc.*, 1975, **97**, 6275–6276.

34 A. Fattahi, L. Lis, Z. Tian and S. R. Kass, *Angew. Chem., Int. Ed.*, 2006, **45**, 4984–4988.
35 J. I. Wu, Y. Mo, F. A. Evangelista and P. v. R. Schleyer, *Chem. Commun.*, 2012, **48**, 8437–8439.
36 C. Hong, J. Baltazar and J. D. Tovar, *Eur. J. Org Chem.*, 2022, **2022**, e202101343.
37 R. Lavendomme and M. Yamashina, *Chem. Sci.*, 2024, **15**, 18677–18697.
38 S. Chakraborty, E. M. Yanes and R. Gershoni-Poranne, *Beilstein J. Org. Chem.*, 2024, **20**, 1817–1830.
39 P. Finkelstein and R. R. Gershoni-Poranne, *ChemPhysChem*, 2019, **20**, 1508–1520.
40 C. S. Anstöter and P. W. Fowler, *ChemPhysChem*, 2025, **26**, e202401069.
41 P. v. R. Schleyer, C. Maerker, A. Dransfeld, H. Jiao and N. J. R. van Eikema Hommes, *J. Am. Chem. Soc.*, 1996, **118**, 6317–6318.
42 C. Corminboeuf, T. Heine and J. Weber, *Phys. Chem. Chem. Phys.*, 2003, **5**, 246–251.
43 D. Flaig, M. Maurer, M. Hanni, K. Braunger, L. Kick, M. Thubauville and C. Ochsenfeld, *J. Chem. Theory Comput.*, 2014, **10**, 572–578.
44 R. Gershoni-Poranne and A. Stanger, *Chem.–Eur. J.*, 2014, **20**, 5673–5688.
45 G. Monaco, F. F. Summa and R. Zanasi, *J. Chem. Inf. Model.*, 2021, **61**, 270–283.
46 T. Gazdag, P. J. Mayer, P. P. Kalapos, T. Holczbauer, O. El Bakouri and G. London, *ACS Omega*, 2022, **7**, 8336–8349.
47 T. Ohmae, T. Nishinaga, M. Wu and M. Iyoda, *J. Am. Chem. Soc.*, 2010, **132**, 1066–1074.
48 T. C. W. Mak and W.-K. Li, *J. Mol. Struct.:THEOCHEM*, 1982, **89**, 281–284.
49 K. K. Baldridge and J. S. Siegel, *J. Am. Chem. Soc.*, 2001, **123**, 1755–1759.
50 A. Matsuura and K. Komatsu, *J. Am. Chem. Soc.*, 2001, **123**, 1768–1769.
51 T. Nishinaga, T. Ohmae and M. Iyoda, *Symmetry*, 2010, **2**, 76–97.
52 K. K. Baldridge and J. S. Siegel, *J. Am. Chem. Soc.*, 2002, **124**, 5514–5517.
53 P. W. Fowler, R. W. A. Havenith, L. W. Jenneskens, A. Soncini and E. Steiner, *Angew. Chem., Int. Ed.*, 2002, **41**, 1558–1560.
54 C. S. Wannere, D. Moran, N. L. Allinger, B. A. Hess, L. J. Schaad and P. v. R. Schleyer, *Org. Lett.*, 2003, **5**, 2983–2986.
55 R. W. A. Havenith, P. W. Fowler and L. W. Jenneskens, *Org. Lett.*, 2006, **8**, 1255–1258.